General analysis of Z^0 decays into lepton pairs and spin-0 bosons

P. Kalyniak, John N. Ng, and P. Zakarauskas
TRIUMF and Physics Department, University of British Columbia, Vancouver, British Columbia, Canada V6T 2A3
(Received 6 September 1983)

We present a general analysis of Z^0 decay into a dilepton pair and a spin-0 particle. Three cases are investigated: the Weinberg-Salam 0^+ Higgs boson, the hypercolor 0^- bosons, and composite 0^+ and 0^- Higgs bosons coupling to composite vector bosons. The density distribution in the two lepton energies, the individual lepton energy spectra, and the distribution in dilepton invariant mass are given. We find the standard Higgs boson to be distinguishable from the other cases studied and also less affected by the main sources of background.

I. INTRODUCTION

Recently the discovery of the Z^0 was made at the CERN SPS $p\bar{p}$ collider;[1] we can now look forward to the discovery of the Higgs boson as a final test of the standard model[2] which utilizes in an essential way the Higgs mechanism for generating masses for both the gauge bosons and fermions. This simplest, although *ad hoc,* procedure receives indirect confirmation in the closeness of the measured value of the ρ parameter[1]

$$\rho \equiv \frac{M_W{}^2}{M_Z{}^2 \cos^2\theta_W} = 0.94 \pm 0.06$$

to the theoretical expected value of Refs. 3 and 4. In turn this renders support to the notion that the Weinberg-Salam Higgs boson exists, possibly as an elementary scalar (0^+) particle.

However, there exists an attractive scheme, namely, the hypercolor or, more generally, extended hypercolor models that employ a dynamical symmetry-breaking mechanism to generate masses.[5] Typically, a host of pseudoscalar (0^-) hyperpions, 0^+ hyper-η, and spin-1 hyperbosons are predicted to exist in these models. The masses of these particles are model dependent; however, the charged hypermesons must have masses greater than 20 GeV/c^2 in order to conform to their nonobservation at DESY PETRA. On the other hand, the limits for the neutral particles are less stringent.

Recently there has also been increasing interest in composite models[6] where the gauge bosons ($W^{\pm}, Z^0$) as well as the scalar bosons (H) are not elementary but rather are made out of the same subconstituents. They have the feature that the $HZ\gamma$ and $H\gamma\gamma$ couplings can be rather large, in contrast to the standard model in which these couplings do not exist at the tree level but can be generated from loop diagrams. Hence, it will be important to examine the testable differences among the various models that use different mechanisms for symmetry breaking and mass generation.

If the Higgs boson or any of the scalar or pseudoscalar bosons in the alternative models lies below the Z^0 mass, then a good signature for their production is via the decay[7–9]

$$Z^0 \to l^+ l^- X^0 , \tag{1.1}$$

where X^0 denotes either the H (Higgs boson), P (hyperpion), CS (composite scalar), or CPS (composite pseudoscalar) boson, and l stands for the electron or muon. In the case of the Higgs boson H, it would then subsequently decay predominantly into the heaviest quark-antiquark (Q and $\bar{Q}$) pairs kinematically allowed, resulting in the signature

$$Z^0 \to l^+ l^- + 2 \text{ jets} . \tag{1.2}$$

A similar signature is expected of the hyperpion P.[10] Thus, both will have a bump in the missing mass recoiling against the dilepton ($l^+ l^-$) pair. To distinguish among the cases of H^0, P^0, P^3, CS, and CPS bosons one has to examine the characteristics of the l^+ and l^- spectra as well as the invariant-mass distribution of the dilepton pair.

In Sec. II we analyze the decay (1.1) in general and indicate the difference between 0^+ and 0^- cases. The only dynamical assumption made here is that one photon and one Z^0 coupling dominate the lepton current (see Fig. 1).

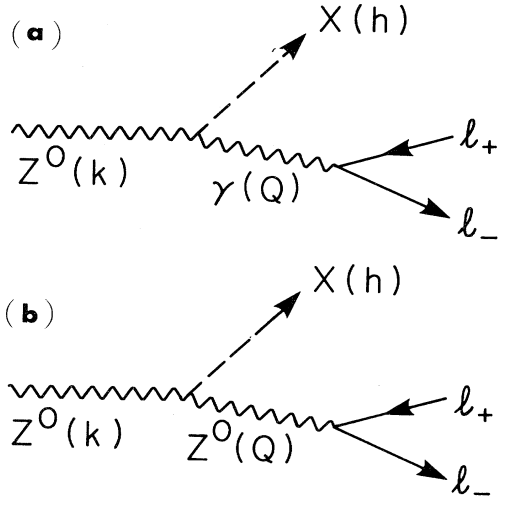

FIG. 1. The decay of Z^0 into a dilepton pair and a spin-0 boson through a virtual (a) photon, (b) Z^0.

In Sec. III we calculate the decay rate for (1.1) and the various spectra of the energies of the l^+ and the l^- for (a) the standard model, (b) the hypercolor model, and (c) a model of composite scalar bosons.[6] The differences between them are displayed for several sample masses of the boson X.

In Sec. IV we summarize our results and indicate which are the best spectra to examine when we want to differentiate between the Higgs boson, hypercolor mesons, and composite particles with masses below M_Z in facilities such as CERN LEP and the Stanford linear collider (SLC). For definiteness we assume $M_Z=93.5$ GeV/c^2 which is the center value measured at the SPS collider.[1]

II. GENERAL ANALYSIS

The total amplitude for the decay of the Z^0 into an l^+l^- pair and a spin-0 meson is given by the Feynman diagram of Figs. 1(a) and 1(b) where the kinematics are defined. We have assumed that the leptonic current is

$$l_\mu^{(\gamma)}=-ie\bar{v}(l_+)\gamma_\mu u(l_-) \tag{2.1}$$

for the photonic contribution of Fig. 1(a) and for the virtual-Z-boson contribution of Fig. 1(b) we use

$$l_\mu^{(Z)}=-i\bar{v}(l_+)(a\gamma_\mu+b\gamma_\mu\gamma_5)u(l_-) \tag{2.2}$$

with

$$a=\frac{g}{\cos\theta_W}(\tfrac{1}{4}-\sin^2\theta_W)\ , \tag{2.3a}$$

$$b=-\frac{g}{4\cos\theta_W} \tag{2.3b}$$

as given by the standard model. We shall assume that if more than one neutral weak boson exists, the additional bosons are heavier than the Weinberg-Salam Z^0 and thus only give nonleading contributions. Furthermore, the leptons that are likely to be directly measurable are muons and electrons. Restricting ourselves to these we can set $m_l=0$ and obtain current conservation for the leptonic vertex, i.e.,

$$l_\mu^{(\gamma)}Q^\mu=0 \tag{2.4a}$$

and

$$l_\mu^{(Z)}Q^\mu\simeq 0 \tag{2.4b}$$

with $Q^\mu\equiv l_+^\mu+l_-^\mu$. We also use the unitary gauge for the Z^0 propagator. The amplitude for the decay (1.1) of a Z^0 with polarization e^μ is given by

$$T=e^\mu(M_{1\mu}+M_{2\mu})\ , \tag{2.5}$$

where

$$M_1^\mu=-\frac{i}{Q^2}l_\nu^{(\gamma)}E_{\gamma Z}^{\mu\nu} \tag{2.6a}$$

and

$$M_2^\mu=\frac{-i}{Q^2-M_Z{}^2}l_\nu^{(Z)}E_{ZZ}^{\mu\nu}\ , \tag{2.6b}$$

where

$$E_{Z\gamma}^{\mu\nu}=\int d^4x\, e^{iQ\cdot x}\langle X\mid T[J_{(Z)}^\mu(x),J_{(\gamma)}^\nu]\mid 0\rangle \tag{2.7a}$$

and

$$E_{ZZ}^{\mu\nu}=\int d^4x\, e^{iQ\cdot x}\langle X\mid T[J_{(Z)}^\mu(x),J_{(Z)}^\nu]\mid 0\rangle \tag{2.7b}$$

with X defined in (1.1). The Lorentz tensors $E_{\gamma Z}^{\mu\nu}$ and $E_{ZZ}^{\mu\nu}$ are constructed out of two independent four-vectors for which we choose the four-momenta of the decaying Z^0, k^μ, and that of the dilepton pair, Q^μ. Using the current-conservation conditions of Eqs. (2.4a) and (2.4b), the contributing terms of the tensors are

$$E_{Z\gamma}^{\mu\nu}=g^{\mu\nu}M_Z{}^2A_1+k^\mu Q^\nu A_2+i\epsilon^{\mu\nu\alpha\beta}k_\alpha Q_\beta A_3+\cdots \tag{2.8a}$$

and

$$E_{ZZ}^{\mu\nu}=g^{\mu\nu}M_Z{}^2B_1+k^\mu Q^\nu B_2+i\epsilon^{\mu\nu\alpha\beta}k_\alpha Q_\beta B_3+\cdots\ , \tag{2.8b}$$

where the decay form factors $A_{1,2,3}$ and $B_{1,2,3}$ are functions of Q^2 and $(k\cdot Q)$ only. The hadronic state X has a definite parity of either even or odd. For $X=0^+$ only the vector part of J_Z^ν contributes to $E_{Z\gamma}$ and both vector-vector and axial-vector—axial-vector components enter into E_{ZZ}. Similarly, only the axial-vector component of J_Z^ν contributes to $E_{\gamma Z}$ and the vector—axial-vector term arises in E_{ZZ} for $X=0^-$. Hence, for the Higgs boson, composite or otherwise (i.e., $X=0^+$),

$$A_3=B_3=0\ , \tag{2.9a}$$

whereas for $X=0^-$ such as the hyperpion, we have

$$A_1=A_2=B_1=B_2=0\ . \tag{2.9b}$$

In the lowest order or at the tree level these form factors will be constants involving the coupling constants such as gauge couplings and masses. However, in general, unknown behavior in Q^2 can occur. A detailed study of the Q^2 dependence of these would involve higher-order corrections to the tree-level couplings. Possible new structures additional to the standard electroweak and strong-interaction picture could be revealed in a careful experimental study of these form factors. We defer to Sec. III discussions of models which are necessary for numerical predictions.

Next we square the amplitude and average over the polarizations of the Z^0 and sum over all spins; we obtain

$$\overline{\sum_{\text{pol}}}\mid M\mid^2=\tfrac{2}{3}\left\{F_1M_Z{}^2[Q^2M_Z{}^2+4(k\cdot l_+)(k\cdot l_-)]+\left[-F_2\left[Q^2-\frac{(k\cdot Q)^2}{M_Z{}^2}\right]+2(k\cdot Q)M_Z{}^2F_4\right][4(k\cdot l_+)(k\cdot l_-)-Q^2M_Z{}^2]\right\} \tag{2.10a}$$

for $X=0^+$ and

$$\sum_{\text{pol}}\overline{|M|^2}=\tfrac{2}{3}F_3Q^2[2(k\cdot Q)^2-Q^2M_Z{}^2-4(k\cdot l_+)(k\cdot l_-)] \tag{2.10b}$$

for $X=0^-$. The functions F_i $(i=1,\ldots,4)$ are defined by

$$F_i=\frac{e^2A_i{}^2}{Q^4}+\frac{(a^2+b^2)B_i{}^2}{(Q^2-M_Z{}^2)^2}+\frac{2aeA_iB_i}{Q^2(Q^2-M_Z{}^2)},\quad i=1,2,3 \tag{2.11}$$

and

$$F_4=\frac{e^2A_1A_2}{Q^4}+\frac{(a^2+b^2)B_1B_2}{(Q^2-M_Z{}^2)^2}+\frac{ea(A_1B_2+A_2B_1)}{Q^2(Q^2-M_Z{}^2)}\ . \tag{2.12}$$

For a Z^0 decaying at rest we calculate the double-differential distribution in the energies of the l^+ and l^- to be

$$\begin{aligned}\frac{d^2R}{dx_+dx_-}=\frac{M_Z{}^3}{384\pi^3}\Bigg\{&\Bigg[\frac{e^2A_1{}^2}{(x_++x_-+\delta^2-1)^2}+\frac{(a^2+b^2)B_1{}^2}{(x_++x_-+\delta^2-2)^2}\\&+\frac{2aeA_1B_1}{(x_++x_-+\delta^2-1)(x_++x_-+\delta^2-2)}\Bigg](x_+x_-+x_++x_-+\delta^2-1)\\&+\Bigg[\Bigg[\frac{e^2A_2{}^2}{(x_++x_-+\delta^2-1)^2}+\frac{(a^2+b^2)B_2{}^2}{(x_++x_-+\delta^2-2)^2}+\frac{2aeA_2B_2}{(x_++x_-+\delta^2-1)(x_++x_-+\delta^2-2)}\Bigg]\\&\times[x_++x_-+\delta^2-1-\tfrac{1}{4}(x_++x_-)^2]\\&-\Bigg[\frac{e^2A_1A_2}{(x_++x_-+\delta^2-1)^2}+\frac{(a^2+b^2)B_1B_2}{(x_++x_-+\delta^2-2)^2}+\frac{ea(A_1B_2+A_2B_1)}{(x_++x_-+\delta^2-1)(x_++x_-+\delta^2-2)}\Bigg]\\&\times(x_++x_-)\Bigg](x_++x_-+\delta^2-1-x_+x_-)\Bigg\}\end{aligned} \tag{2.13a}$$

for the $X=0^+$ boson whereas

$$\begin{aligned}\frac{d^2R}{dx_+dx_-}=\frac{M_Z{}^3}{384\pi^3}&\Bigg[\frac{e^2A_3{}^2}{(x_++x_-+\delta^2-1)}+\frac{(a^2+b^2)B_3{}^2(x_++x_-+\delta^2-1)}{(x_++x_-+\delta^2-2)^2}+\frac{2aeA_3B_3}{(x_++x_-+\delta^2-2)^2}\Bigg]\\&\times[\tfrac{1}{2}(x_+{}^2+x_-{}^2)-(x_++x_-+\delta^2-1)]\end{aligned} \tag{2.13b}$$

for the $X=0^-$ boson.

In Eqs. (2.13a) and (2.13b) we have used the reduced energies of the leptons defined by

$$x_\pm\equiv\frac{2E_\pm}{M_Z} \tag{2.14}$$

and the reduced mass

$$\delta\equiv\frac{M_X}{M_Z}\ . \tag{2.15}$$

The limits of x_+ and x_- are given by the Dalitz contour which is

$$-x_+x_-\le 1-x_+-x_--\delta^2\le 0 \tag{2.16}$$

in the limit of massless leptons.

Both of the differential rates, Eqs. (2.13a) and (2.13b), are symmetrical under the interchange of x_+ and x_- and we also note that the form factors as defined have dimensions of inverse mass. To proceed further we need more dynamical assumptions on the form factors; this we shall do in Sec. III.

III. MODEL CALCULATIONS

A. Glashow-Weinberg-Salam model

In this model the only relevant tree-level coupling for the decay (1.1) is the ZZH vertex. Hence, only the Feynman graph of Fig. 1(b) gives the leading contribution, and the other graph enters only when higher-order effects are needed. The form factors at the tree level are

$$A_1=A_2=B_2=0 \tag{3.1}$$

and

$$B_1=\frac{g}{M_Z\cos\theta_W}\ . \tag{3.2}$$

The double-differential decay rate simplifies to[9]

$$\frac{dR}{dx_+dx_-}=\frac{M_Z{}^3}{384\pi^3}(a^2+b^2)\left[\frac{g^2}{M_Z{}^2\cos^2\theta_W}\right]\times\frac{x_++x_-+\delta^2-1+x_+x_-}{(x_++x_-+\delta^2-2)^2}, \tag{3.3}$$

which after integration gives the branching ratio of $Z^0\to l^+l^-H^0$. This is typically of the order of 10^{-5}. In Table I we give the decay rate for several values of δ. Our results agree with the rate estimate given in Ref. 9. In parts (i) and (ii) of Fig. 2(a) we present the density plots in x_+ and x_- of the decay spectra for $\delta=0.2$ and 0.5, respectively. It is seen that the events are populated more

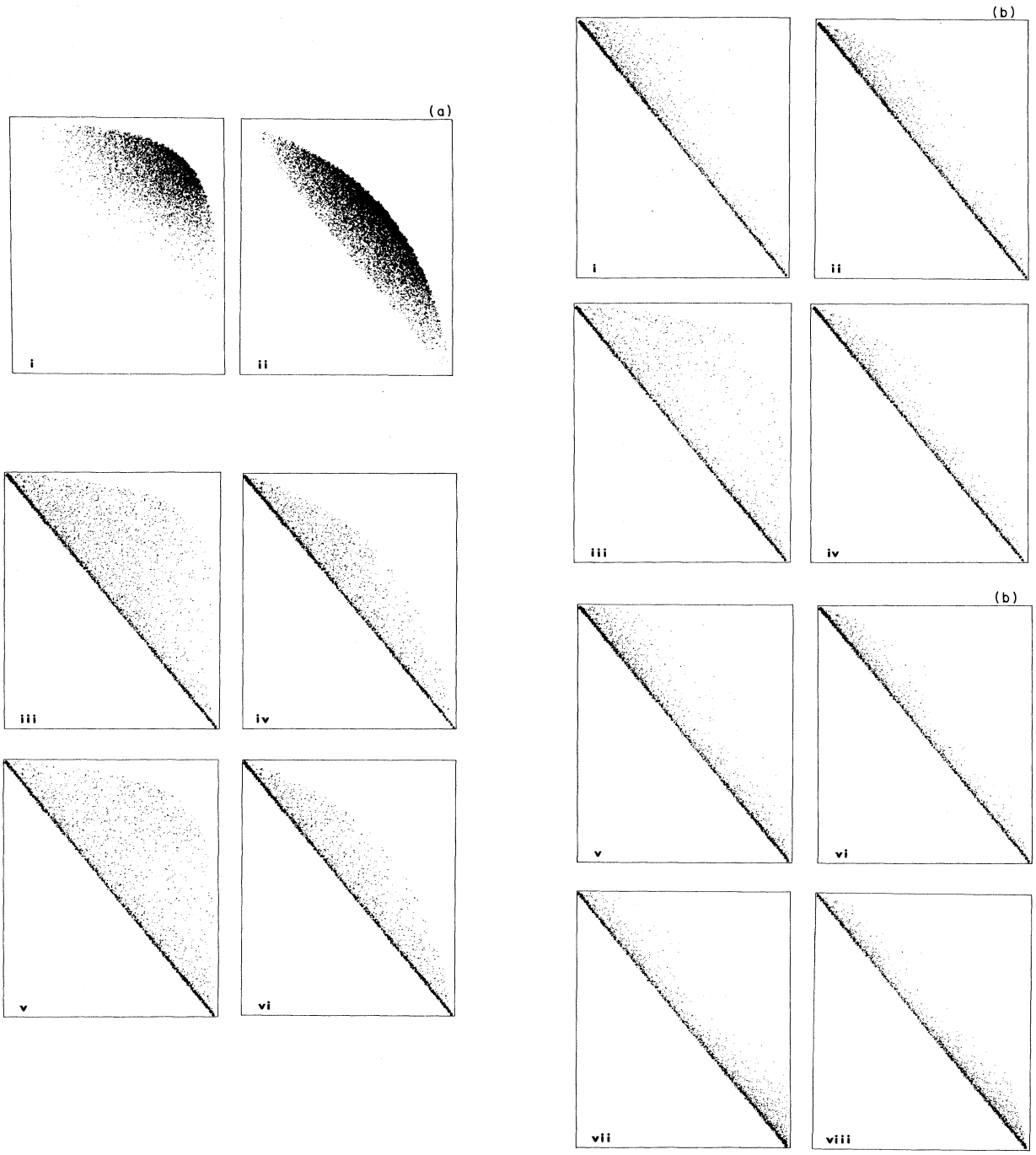

FIG. 2. The density distribution in x_+ and x_- for decay into (a) 0^+ boson: standard Higgs boson for $\delta=0.2$ (i) and 0.5 (ii); CS with dominant $HZ\gamma$ coupling for $\delta=0.2$ (iii) and 0.5 (iv); CS with comparable $HZ\gamma$ and HZZ couplings for $\delta=0.2$ (v) and 0.5 (vi). (b) 0^- boson: P^0 for $\delta=0.2$ (i) and 0.5 (ii); P^3 for $\delta=0.2$ (iii) and 0.5 (iv); CPS with dominant $HZ\gamma$ coupling for $\delta=0.2$ (v) and 0.5 (vi); CPS with comparable $HZ\gamma$ and HZZ couplings for $\delta=0.2$ (vii) and 0.5 (viii).

TABLE I. Decay rate of $Z^0 \to l^+ l^- X^0$ in units of GeV for (a) the Weinberg-Salam model, (b) the hypercolor model with SU(4) hypercolor group, and (c) the composite-gauge-boson model. C^1 is the composite model with photon-pole dominance and C^2 is the model with both photon and Z^0 couplings. The value of the weak mixing angle used is $\sin^2\theta_W = 0.23$, and $M_Z = 93.5$ GeV/c^2.

		Hypercolor		C^1		C^2	
δ	Weinberg-Salam	P^0	P^3	0^+	0^-	0^+	0^-
0.05	4.9×10^{-4}	3.4×10^{-9}	9.8×10^{-8}	4.8×10^{-6}	4.3×10^{-6}	5.4×10^{-6}	4.4×10^{-6}
0.2	7.6×10^{-5}	3.0×10^{-9}	4.5×10^{-10}	4.2×10^{-6}	3.8×10^{-6}	4.4×10^{-6}	3.8×10^{-6}
0.5	5.5×10^{-6}	1.4×10^{-9}	1.6×10^{-10}	1.9×10^{-6}	1.7×10^{-6}	1.9×10^{-6}	1.8×10^{-6}
0.75	1.8×10^{-7}	2.6×10^{-10}	2.4×10^{-11}	3.4×10^{-7}	3.2×10^{-7}	3.5×10^{-7}	3.2×10^{-7}

along the upper curve of the Dalitz contour, and most dense in the central region of that curve. Useful information is also contained in the energy spectrum of either the l^+ or l^-. Since they are symmetrical one does not expect any difference between their individual spectra. For the Higgs model we have

$$\frac{dR}{dx_\pm} = \frac{M_Z^3}{384\pi^3}(a^2+b^2)\frac{g^2}{M_Z^2\cos^2\theta_W}\left[-2+x_\pm^2+x_\pm(\delta^2-1)+\frac{2(1-x_\pm)}{1+x_\pm^2+x_\pm(\delta^2-2)} + (1+x_\pm)\ln\left[\frac{1+x_\pm^2+x_\pm(\delta^2-2)}{1-x_\pm}\right]\right]. \tag{3.4}$$

This is shown in Figs. 3(a) and 3(b) for $\delta=0.2$ and 0.5, respectively. Each spectrum peaks towards the high-energy end.

Also, we find the invariant-mass distribution of the lepton pair to be

$$\frac{dR}{d\kappa^2} = \frac{M_Z(a^2+b^2)g^2}{576\pi^3\cos^2\theta_W}\frac{\lambda(1,\delta^2,\kappa^2)}{(\kappa^2-1)^2}\left[3\kappa^2+\tfrac{1}{4}\lambda^2(1,\delta^2,\kappa^2)\right], \tag{3.5}$$

where

$$\lambda(x,y,z) = (x^2+y^2+z^2-2xy-2xz-2yz)^{1/2} \tag{3.6}$$

and

$$\kappa^2 \equiv \frac{Q^2}{M_Z^2}. \tag{3.7}$$

This distribution is presented in Figs. 4(a) and 4(b) for $\delta=0.2$ and 0.5, respectively. The distribution peaks at the high-κ^2 end.

B. Hypercolor models[5,9,10]

In these models the resonance X can be either a hyperpion P^0 or P^3 with odd parity or a hyper-δ with even parity. It is expected that the latter will be heavier than the P^0 and will not be the first contribution to the decay of (1.1). To the lowest order, the form factors for $X=P^0$ and P^3 are given by

$$A_1 = A_2 = B_1 = B_2 = 0 \tag{3.8}$$

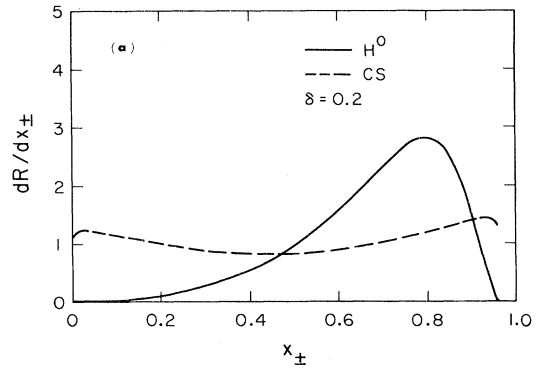

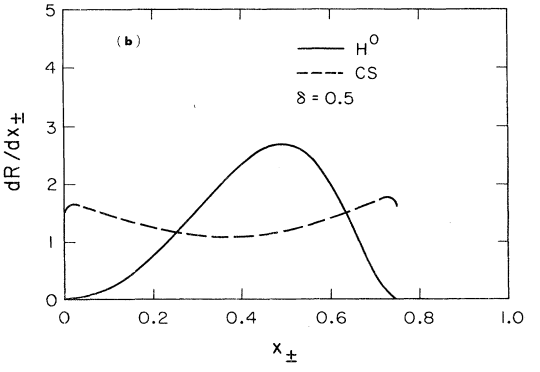

FIG. 3. The distribution in $x_\pm$ for 0^+ bosons with (a) $\delta=0.2$ and (b) $\delta=0.5$. The solid curve represents $X=H^0$; the dashed curve represents $X=$CS, dominant $HZ\gamma$ coupling and comparable $HZ\gamma$ and HZZ couplings being indistinguishable.

and

$$A_3=\begin{cases}\dfrac{\alpha}{9\pi f_{\pi'}}g_{A'}\tan\theta_W N_{c'}n_{F'} \quad (X=P^0)\,, \\ \dfrac{\alpha}{6\pi f_{\pi'}}g_{A'}\dfrac{1-4\sin^2\theta_W}{\sin 2\theta_W}N_{c'}n_{F'} \quad (X=P^3)\,,\end{cases} \tag{3.9}$$

$$B_3=\begin{cases}-\dfrac{\alpha}{9\pi f_{\pi'}}g_{A'}\tan^2\theta_W N_{c'}n_{F'} \quad (x=P^0)\,, \\ -\dfrac{2\alpha}{3\pi f_{\pi'}}g_{A'}\dfrac{(1-2\sin^2\theta_W)\sin^2\theta_W}{(\sin 2\theta_W)^2}N_{c'}n_{F'} \quad (X=P^3)\,,\end{cases} \tag{3.10}$$

where $N_{c'}$ is the number of hypercolors, $g_{A'}\approx 1$ is the hyperquark analog of g_A, $f_{\pi'}$ is the hyperpion decay constant, and $n_{F'}$ is the number of hyperquark doublets. Clearly this class of model contains a large number of unknown parameters. As pointed out in Ref. 9 the branching ratio of Z^0 into P^0 or P^3 is small compared to the decay mode into the Higgs boson unless one or more of the parameters $N_{c'}$, $n_{F'}$, etc., is large. In the second column of Table I we give the branching ratio for the values of $N_{c'}=3$ and $N_{F'}=3$ as illustrative examples only.

The scatter plot in x_+ and x_- is given by Eq. (2.13b) with Eqs. (3.8)—(3.10) substituted in. We compare this with the case of $X=H^0$ for the same values of δ and this is shown in parts (i)—(iv) of Fig. 2(b). All of our differential cross sections are normalized to the same (arbitrary) value. The distributions for P^0 and P^3 are seen to be very different from that of the H^0 case. Whereas the Higgs-boson distribution was most dense in the central region of the upper curve of the Dalitz boundary, and minimal along the lower boundary, the hyperpion distributions are opposite. These distributions are maximal along the lower line of the Dalitz contour, peaking at the upper and lower limits of the lepton energies. This behavior is a result of the dominance of the $HZ\gamma$ coupling, which is absent in the Higgs-boson case at the tree level.

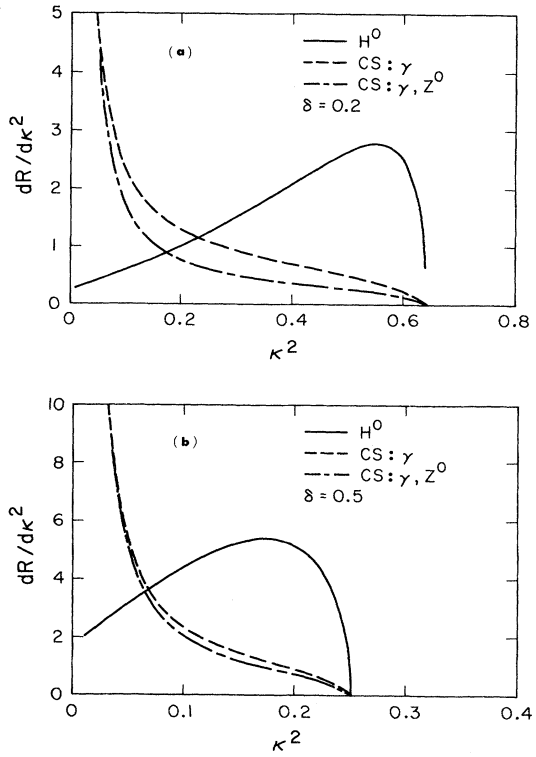

FIG. 4. The dilepton invariant-mass distribution for 0^+ bosons with (a) $\delta=0.2$ and (b) $\delta=0.5$. The solid curve represents $X=H^0$. The dashed curve represents $X=$CS with dominant $HZ\gamma$ coupling and the dash-dot curve is for $X=$CS with comparable $HZ\gamma$ and HZZ couplings.

The single-particle energy distributions for the hypercolor mesons are given by

$$\begin{aligned}\frac{dR}{dx_\pm}=\frac{M_Z{}^3}{384\pi^3}\Bigg\{&e^2A_3{}^2\left[\tfrac{1}{2}[(\delta^2-1)^2+2x_\pm{}^2+2x_\pm(\delta^2-1)]\ln\left[\frac{-x_\pm(\delta^2-1+x_\pm)+2\delta_e{}^2}{2\delta_e{}^2(1-x_\pm)}\right]\right.\\&\left.-\frac{x_\pm}{2}(\delta^2+x_\pm-1)\frac{1-\delta^2-x_\pm+2\delta_e{}^2}{1-x_\pm}+\frac{x_\pm(1-\delta^2-x_\pm+2\delta_e{}^2)^2(2-x_\pm)}{4(1-x_\pm)^2}\right]\\&+aeA_3B_3\left[[(\delta^2-2)^2+2x_\pm(\delta^2-2)+2x_\pm{}^2-2]\ln\left[\frac{x_\pm(\delta^2-2+x_\pm)+1}{1-x_\pm}\right]\right.\\&\left.-\frac{x_\pm(\delta^2+x_\pm)(1-\delta^2-x_\pm)}{1-x_\pm}+\frac{x_\pm(1-\delta^2-x_\pm)^2(2-x_\pm)}{2(1-x_\pm)^2}\right]\\&+(a^2+b^2)B_3{}^2\left[\tfrac{1}{2}[(\delta^2-2)^2+2x_\pm(\delta^2-2)+2x_\pm{}^2-2]\left[\frac{1-x_\pm}{x_\pm(\delta^2-2+x_\pm)+1}-1\right]\right.\\&+\{\tfrac{1}{2}[(\delta^2-2)^2+2x_\pm(\delta^2-2)+2x_\pm{}^2-2]+1-\delta^2-x_\pm\}\ln\left[\frac{x_\pm(\delta^2-2+x_\pm)+1}{1-x_\pm}\right]\\&\left.\left.+\frac{x_\pm(1-\delta^2-x_\pm)^2}{2(1-x_\pm)}+\frac{x_\pm(1-\delta^2-x_\pm)^2(2-x_\pm)}{(1-x_\pm)^2}\right]\right\}.\end{aligned} \tag{3.11}$$

In Figs. 5(a) and 5(b) we display them for $\delta=0.2$ and 0.5, respectively. We see that the distributions in $x_\pm$ are quite different for the Higgs-boson and hyperpion cases. As we noted earlier, the Higgs-boson $x_\pm$ distribution peaks towards the upper-$x_\pm$ end. The hyperpion $x_\pm$ distributions are much flatter for small δ and develop a dip, peaking towards the lower and upper limits of $x_\pm$, as δ increases.

Also, a pronounced difference between the Higgs-boson and hyperpion cases is discerned in the reduced invariant-mass distribution of the dilepton pair. For the odd-parity hypermesons we have

$$\frac{dR}{d\kappa^2}=\frac{M_Z{}^3}{576\pi^3}\lambda^3(1,\delta^2,\kappa^2)\left[\frac{e^2A_3{}^2}{\kappa^2}+\frac{(a^2+b^2)B_3{}^2\kappa^2}{(\kappa^2-1)^2}+\frac{2aeA_3B_3}{\kappa^2-1}\right], \tag{3.12}$$

where λ and κ^2 are given in Eqs. (3.6) and (3.7), respectively. This is plotted for $\delta=0.2$ and 0.5 in Figs. 6(a) and 6(b), respectively. We see that the decay into a hyperpion favors lower values of κ^2 whereas for $X=H^0$ of the same mass higher values of κ^2 are preferred. The Higgs-boson case is due to the Z^0-pole dominance; thus, $\kappa^2\to 1$ is favored. On the other hand, for P^0 and P^3, the $1/\kappa^2$ (photon-pole) term of the distribution completely dominates at low κ^2. The kinematic factor λ^3 largely washes out any effect of the Z^0-pole terms that behave as $(\kappa^2-1)^{-1}$. Thus, the hyperpion distributions exhibit very strong peaking at the low-κ^2 end. The P^0 distribution falls rather more rapidly than that of P^3. We note here that our results are good to the lowest order. Effects of the kind $Q^2/\Lambda_{HC}{}^2$, where Λ_{HC} is the hypercolor scale parameter, are not included. Since these effects are of higher order they are expected to be small. They further involve unknown functional behavior of the form factors which we will not venture to speculate on.

C. Composite models

As in the case of hypercolor models, we will be content with extracting the pointlike couplings for $H\gamma Z$ and HZZ vertices. Terms of the order of $Q^2/\Lambda_c{}^2$, where Λ_c is the energy scale for the manifestation of compositeness, are expected to be small and will be neglected. The current observations of the W and Z at the expected masses indicate that Λ_c is at least greater than 1 TeV.

To be specific we use the considerations of this class of models given in Ref. 6. There is no preference in the parities for the lowest lying spin-0 mesons and we will treat them equally.

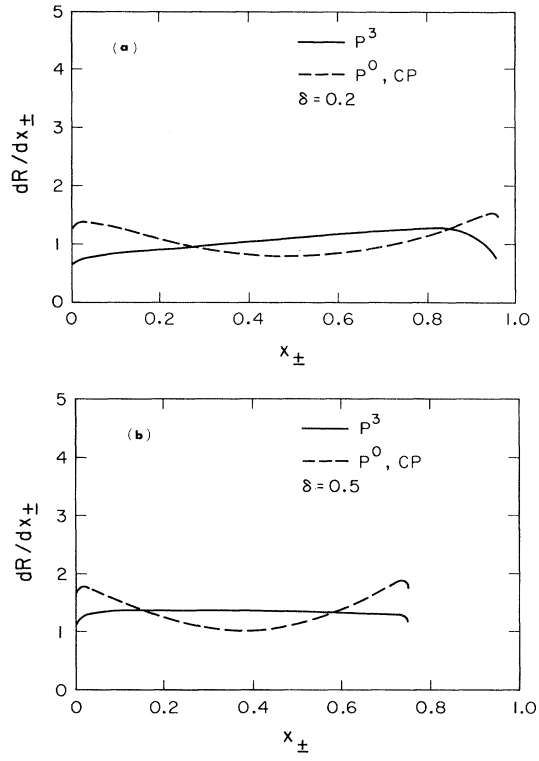

FIG. 5. The distribution in $x_\pm$ for 0^- bosons with (a) $\delta=0.2$ and (b) $\delta=0.5$. The solid curve represents $X=P^3$; the dashed curve represents $X=P^0$ and CPS with dominant $HZ\gamma$ coupling or comparable $HZ\gamma$ and HZZ couplings.

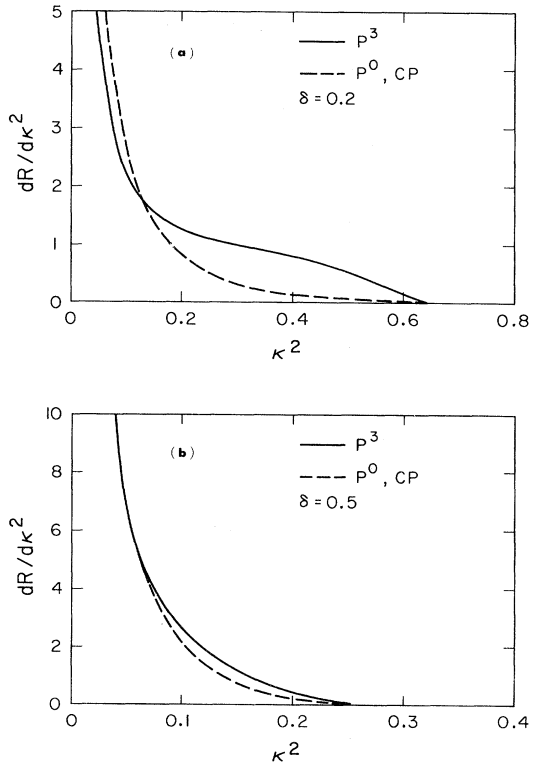

FIG. 6. The dilepton invariant-mass distribution for 0^- bosons with (a) $\delta=0.2$ and (b) $\delta=0.5$. The solid curve represents $X=P^3$; the dashed curve represents $X=P^0$ and CPS with dominant $HZ\gamma$ coupling or comparable $HZ\gamma$ and HZZ couplings.

Both $H\gamma Z$ and HZZ couplings can contribute in the lowest order to the decay (1.1). Their relative strength depends very much on the specifics of the dynamical assumptions such as whether vector-boson dominance is operative. We shall be phenomenological and investigate the case of $H\gamma Z$ being the dominant coupling as well as the case with $H\gamma Z$ and HZZ comparable. The former is of marked contrast to the Higgs-boson case where HZZ is the only operative term at the tree level. Obviously, for composite models where the HZZ is the dominant coupling, to lowest order there is no discernible difference compared to the standard elementary Higgs boson. To look for differences one has to compare higher-order Q^2-dependence effects. Composite models are currently not restrictive enough to do this meaningfully.

Returning to the case of dominant $H\gamma Z$ coupling in composite models we write for $X=0^+$

$$A_2=f_{H\gamma Z},\quad A_1=-\tfrac{1}{2}(x_++x_-)f_{H\gamma Z} \tag{3.13}$$

and the rest of the form factors are zero. The quantity $f_{H\gamma Z}$ is an overall normalizing factor and depends on Λ_c. Approximately, $f_{H\gamma Z}\sim e/\Lambda_c$ and we have chosen Λ_c to be 1 TeV for our numerical estimates in Table I.

Similarly, for $X=0^-$, only A_3 contributes and it is given by

$$A_3=f_{H\gamma Z}\ . \tag{3.14}$$

The appropriate formulas for the scatter plot can be read from the general Eqs. (2.13a) and (2.13b) with obvious changes in the form factors as required by Eqs. (3.13) and (3.14).

For the CS, the effects of the photon-pole dominance in the decay (1.1) are revealed in the scatter plot of x_+ and x_-, shown in parts (iii) and (iv) of Fig. 2(a), for $\delta=(0.2,0.5)$, respectively. We see a marked distinction in comparing the 0^+ composite-Higgs-boson distribution with that of the elementary-Higgs-boson case of parts (i) and (ii) of Fig. 2(a). Here the events are strongly clustered along the lower curve of the Dalitz contour. For the 0^+ composite Higgs boson, the distribution is most dense in the central region of the lower curve. The energy spectrum of either the l^+ or l^- for decays into a CS boson is given below:

$$\begin{aligned}
\frac{dR}{dx_\pm}=\frac{M_Z{}^3}{192\pi^3}\Bigg\{&\frac{e^2\tilde{A}_1{}^2}{2}\Bigg[(1-\delta^2)\{1-\delta^2+x_\pm[3(1-\delta^2)-2x_\pm]\}\ln\left[\frac{x_\pm(1-\delta^2-x_\pm)+2\delta_l{}^2}{2\delta_l{}^2(1-x_\pm)}\right]\\
&+\frac{x_\pm(1-\delta^2-x_\pm)}{1-x_\pm}\left[2(1-\delta^2)+x_\pm[3(1-\delta^2)-x_\pm]+\frac{x_\pm(1+x_\pm)(1-\delta^2-x_\pm)}{2(1-x_\pm)}\right]\\
&-(1-\delta^2)^2\left[1-x_\pm-\frac{x_\pm(1-\delta^2-x_\pm)}{2\delta_l{}^2}\right]\Bigg]\\
&+\frac{(a^2+b^2)B_1{}^2}{2}\left[(1+x_\pm)\ln\left[\frac{x_\pm(x_\pm+\delta^2-2)+1}{1-x_\pm}\right]-[1+(2-\delta^2)x_\pm-x_\pm{}^2]\left[1+\frac{1-x_\pm}{x_\pm(2-x_\pm-\delta^2)-1}\right]\right]\\
&+ae\tilde{A}_1B_1\Bigg[(2-\delta^2)[1+x_\pm(2-\delta^2-x_\pm]\ln\left[\frac{x_\pm(x_\pm-\delta^2+2)+1}{1-x_\pm}\right]\\
&+\frac{x_\pm(1+2x_\pm)(1-\delta^2-x_\pm)}{1-x_\pm}+x_\pm(1-\delta^2)(x_\pm+\delta^2-1)\ln\left[\frac{x_\pm(1-\delta^2-x_\pm)+2\delta_l{}^2}{2\delta_l{}^2(1-x_\pm)}\right]\\
&+\frac{x_\pm{}^2(1-\delta^2-x_\pm)}{2(1-x_\pm)^2}[-x_\pm(1-\delta^2-x_\pm)+3x_\pm-2-x_\pm{}^2-x_\pm\delta^2]\Bigg]\\
&+\frac{e^2A_2{}^2}{2}\Bigg[\frac{x_\pm(1-\delta^2-x_\pm)}{1-x_\pm}\left[1-\tfrac{1}{4}\{2(2x_\pm-\delta^2+1)-x_\pm[3(1-\delta^2)-x_\pm\}-\frac{x_\pm(1-\delta^2-x_\pm)}{8}\right]\\
&-\tfrac{1}{4}\{4x_\pm(1-\delta^2-x_\pm)+(\delta^2-1)^2-x_\pm(1-\delta^2)[3(1-\delta^2)-2x_\pm]\}\ln\left[\frac{x_\pm(1-\delta^2-x_\pm)+2\delta_l{}^2}{2\delta_l{}^2(1-x_\pm)}\right]\\
&-\frac{(1-\delta^2)}{4^2}\left[1-x_\pm-\frac{x_\pm(1-\delta^2-x_\pm)}{2\delta_l{}^2}\right]\Bigg]\\
&+\frac{e^2\tilde{A}_1A_2}{2}\Bigg[(1-\delta^2)\{\delta^2-1+x_\pm[3(1-\delta^2)-2x_\pm]\}\ln\left[\frac{x_\pm(1-\delta^2-x_\pm)+2\delta_l{}^2}{2\delta_l{}^2(1-x_\pm)}\right]\\
&+\frac{x_\pm(1-\delta^2-x_\pm)}{1-x_\pm)}\left[-2(1-\delta^2)+x_\pm[3(1-\delta^2)-x_\pm]-\frac{x_\pm}{2}(1-\delta^2-x_\pm)\right]
\end{aligned}$$

$$-(1-\delta^2)^2\left[1-x_\pm-\frac{x_\pm(1-\delta^2-x_\pm)}{2\delta_l{}^2}\right]\Bigg]$$

$$+\frac{aeA_2B_1}{2}\left[(\delta^2-2)[1+x_\pm(x_\pm+\delta^2-2)]\ln\left[\frac{x_\pm(x_\pm+\delta^2-2)+1}{1-x_\pm}\right]\right.$$

$$\left.+\,x_\pm(1-\delta^2)(x_\pm+\delta^2-1)\ln\left[\frac{x_\pm(1-\delta^2-x_\pm)+2\delta_l{}^2}{2\delta_l{}^2(1-x_\pm)}\right]-x_\pm(1-\delta^2-x_\pm)\right]\Bigg\}. \tag{3.15}$$

Here, with the dominant $H\gamma Z$ coupling

$$\delta_l\equiv\frac{m_l}{M_Z}\ , \tag{3.16}$$

and $\tilde{A}_1$ is defined by

$$A_2=f_{H\gamma Z}=-2\tilde{A}_1\ , \tag{3.17}$$

while the other couplings are set equal to zero. The distribution for the two values of $\delta=0.2$ and 0.5 are shown, along with the standard-Higgs-boson case, in Figs. 3(a) and 3(b), respectively. Here the spectrum is rather flat with slight peaking at the lower and upper limits of $x_\pm$, whereas the spectrum for the standard-Higgs-boson case peaks toward large $x_\pm$.

Another contrast of the two cases is presented in the κ^2 distribution. For the 0^+ composite Higgs boson, this distribution is

$$\frac{dR}{d\kappa^2}=\frac{M_Z{}^3}{192\pi^3}\lambda(1,\delta^2,\kappa^2)\left[\left[\frac{e^2A_1{}^2}{\kappa^4}+\frac{(a^2+b^2)B_1{}^2}{(\kappa^2-1)^2}+\frac{2aeA_1B_1}{\kappa^2(\kappa^2-1)}\right]\{\kappa^2+\tfrac{1}{3}[\tfrac{1}{2}(1-\delta^2+\kappa^2)^2+\kappa^2]\}\right.$$

$$+\left[\frac{e^2A_2{}^2}{\kappa^4}+\frac{(a^2+b^2)B_2{}^2}{(\kappa^2-1)^2}+\frac{2aeA_2B_2}{\kappa^2(\kappa^2-1)}\right]\tfrac{1}{4}(3\kappa^2+\delta^2-1)\{\kappa^2-\tfrac{1}{3}[\tfrac{1}{2}(1-\delta^2+\kappa^2)^2+\kappa^2]\}$$

$$+\left[e^2\frac{A_1A_2}{\kappa^4}+\frac{(a^2+b^2)B_1B_2}{(\kappa^2-1)^2}+ae\frac{A_1B_2+A_2B_1}{\kappa^2(\kappa^2-1)}\right](1-\delta^2+\kappa^2)$$

$$\left.\times\{-\kappa^2+\tfrac{1}{3}[\tfrac{1}{2}(1-\delta^2+\kappa^2)^2+\kappa^2]\}\right]\ , \tag{3.18}$$

where

$$A_1=\tfrac{1}{2}(-1+\delta^2-\kappa^2)f_{HZ\gamma}\ . \tag{3.19}$$

For the dominant $H\gamma Z$ case ($B_1=B_2=0$), the distribution is given in Figs. 4(a) and 4(b) for $\delta=0.2$ and 0.5, respectively. For all δ, $dR/d\kappa^2$ rises towards the low-κ^2 end similar to the hyperpion case although this refers to a 0^+ meson. This illustrates the effects of the photon-pole dominance of the model under consideration.

Next we can compare the CPS boson in composite models with photon dominance with the hyperpion case by looking at the Dalitz plot. For the CPS boson the population of events is most dense along the lower curve of the Dalitz plot and peaks at the tip ends of the x_+ and x_- limits; parts (v) and (vi) of Fig. 2(b) for $\delta=0.2$ and 0.5, respectively. This is, of course, very similar to the hyperpion case.

For the CPS, the distribution in energy of l_+ or l_- is given by Eq. (3.11) with the substitution of Eq. (3.14) for the coupling. The spectra are shown in Figs. 5(a) and 5(b) for $\delta=0.2$ and 0.5, respectively, along with the spectra for P^0 and P^3. The distribution in $x_\pm$ for the cases of a CPS boson with photon dominance and P^0 are *indistinguishable.*

The differential distribution in κ^2 is the same as that for the hyperpion, Eq. (3.12), with the appropriate form factors and A_1 given by Eq. (3.19). The κ^2 dependence also reflects the assumption of photon-pole dominance in that the locale of the peak has shifted towards low values of κ^2. The CPS case is indistinguishable from that of P^0.

Lying between photon dominance and the standard model is the case where $H\gamma Z$ and HZZ are of comparable strength. We choose the HZZ coupling given by the scale of compositeness and the $HZ\gamma$ coupling of the last example:

$$A_1=-\tfrac{1}{2}(x_++x_-)f_{H\gamma Z}\ , \tag{3.20}$$

$$B_1=f_{H\gamma Z}\ . \tag{3.21}$$

For $X=0^-$, we use

$$A_3=f_{H\gamma Z}\ , \tag{3.22}$$

$$B_3=f_{H\gamma Z}\ . \tag{3.23}$$

The scatter-plot distributions, shown in parts (v) and (vi) of Fig. 2(a) for the 0^+ and in parts (vii) and (viii) of Fig. 2(b) for the 0^-, are very similar to their respective photon-pole-dominance scatter distributions. The distributions in energy of either l^+ or l^- are given by Eq. (3.15) for the CS and (3.12) for the CPS with the couplings given above. The CS case is plotted in Figs. 3(a) and 3(b) for $\delta=0.2$ and 0.5, respectively, together with the standard-Higgs-boson case and the CS-with-dominant-$HZ\gamma$-coupling case. This case is indistinguishable from the dominant-$HZ\gamma$-coupling case. The same is true for the CPS boson which is plotted in Figs. 5(a) and 5(b) for $\delta=0.2$ and 0.5.

For the 0^+ composite Higgs boson, the $dR/d\kappa^2$ distribution, Eq. (3.18), becomes similar to the hyperpion behavior for all values of δ since A_2 is zero in our coupling scheme. The distributions in κ^2 for the CS boson are shown in Figs. 4(a) and 4(b) for $\delta=0.2$ and 0.5, respectively. The 0^- composite has a distribution in κ^2 indistinguishable from that of the dominant $HZ\gamma$ coupling case and of P^0. See Figs. 6(a) and 6(b) for $\delta=0.2$ and 0.5, respectively.

IV. CONCLUSION

We have performed a general analysis of Z^0 decay into a dilepton pair and a spin-0 particle. The experimentally measurable quantities which we have calculated are the scatter-plot distribution in the two lepton energies, the individual lepton energy spectra, and the distribution in dilepton invariant mass squared, κ^2. These quantities were investigated for three general types of the spin-0 particle: the usual Weinberg-Salam 0^+ Higgs boson, the hypercolor 0^- bosons (hyperpions), and a composite Higgs boson (0^+ and 0^-) coupling to composite vector bosons. More generally we find that the decay (1.1) is a sensitive test of the couplings XZZ and $X\gamma Z$. For the standard-Higgs-boson case, only the ZZH coupling contributes at the tree level. The two hyperpions, P^0 and P^3, of the hypercolor models have both HZZ and $H\gamma Z$ couplings. These couplings, given in Sec. III, are calculated at the one-loop level which is the lowest order for the hypercolor models. For the case of composite models with the Higgs boson and the vector mesons built of the same constituents, substantial $HZ\gamma$ couplings are possible, in contrast to the standard-Higgs-boson case. We investigated the case of $HZ\gamma$ coupling dominance and the case wherein $HZ\gamma$ and HZZ couplings were comparable, and have approximately the same strength as the HZZ coupling in the standard-Higgs-boson case.

We find the models to be generally distinguishable using the different experimental signatures considered here. We will summarize these below:

(a) *The x_+x_- distribution.* The scatter plots in x_+ and x_- are given in Figs. 2(a) and 2(b) comparing the various types of spin-0 particles of the same mass. The standard-Higgs-boson distribution is very different from the others, being most dense in the central region of the upper curve of the Dalitz plot. All the other cases cluster most densely along the lower curve of the Dalitz boundary, reflecting the photon pole of the $HZ\gamma$ coupling, absent in the standard-Higgs-boson case. The 0^+ composite scalar peaks towards the central region of the lower curve, whereas the Higgs boson peaked towards the center of the upper curve. The 0^- cases, P^0, P^3, and composite pseudoscalars, have their most dense distribution towards the upper and lower $x_\pm$ limits of the lower line of the Dalitz boundary. Thus, Z^0-pole dominance separates the standard-Higgs-boson case from the others, while 0^+ and 0^- cases are also distinguishable. Of course, a CS with HZZ coupling only would have a distribution very similar to that of the Higgs boson. That will be very unlikely without invoking accidental vanishing of the photon term.

(b) *The distributions in $x_\pm$.* These are quite different for the standard-Higgs-boson and the other cases. The Higgs-boson distribution peaks towards the upper end of the spectrum. The P^3 distribution is much flatter; for values of $\delta \gtrsim 0.6$, the spectrum develops a dip while the Higgs-boson spectrum is strongly peaked. The P^0 and composite-Higgs-boson distributions calculated all have slight peaking at the upper and lower limits of $x_\pm$, indistinguishable from each other.

(c) *The invariant mass squared of the dileptons.* Here the Higgs-boson and hyperpion models are easily separable. The Higgs-boson distribution peaks towards high κ^2 reflecting the Z^0 pole while the hyperpion distribution peaks at the low-κ^2 end. As discussed in Sec. III B, the kinematic factor λ^3 in the κ^2 distribution for the hyperpions enhances the peaking at the low-κ^2 end. The 0^- CPS has a κ^2 distribution very similar to that of the hyperpion; only differences in the choice of A_3 and B_3 distinguish them and these are, after all, phenomenological. The 0^+ CS with comparable γ and Z^0 coupling strength has a distribution quite similar to the hyperpion. For the photon-pole-dominance case, the 0^+ composite distribution rises towards low κ^2 resembling the hyperpion case as well. Again, we emphasize that couplings were chosen arbitrarily to investigate various possibilities.

Branching ratios are given for each of the models for several values of δ in Table I. In this table, we have chosen $N_{c'}=3$ and $n_{F'}=3$. For this choice the branching ratio into hyperpions is down from that into the standard Higgs boson by a factor of about 10^4. However, even if the values of $N_{c'}$ and $n_{F'}$ were large, the decay of Z^0 into hyperpions would be distinguishable from the decay to Higgs boson in the κ^2 or $x_\pm$ distributions. The branching ratio for the decay into the composite Higgs boson can be made comparable to that into the elementary Higgs boson. However, distinguishing this from the hypercolor mesons would only be possible with high statistics using the $x_\pm$ or scatter plot in x_+ and x_-.

Next we discuss briefly the background to this decay mode.[8,11,12] Two major sources can be identified; namely, the two-photon interactions,

$$e^+e^- \to l^+l^- + 2 \text{ quark jets} , \tag{4.1}$$

at the resonance, and higher-order Z^0 decay,

$$Z^0 \to l^+l^- + 2 \text{ quark jets} . \tag{4.2}$$

These can be seen by power counting and including the

logarithmic enhancement factors in powers of $\ln(m_Z/m_e)$ to give a branching ratio of approximately 10^{-4} for $l=e$. However, the κ^2 distributions of the dilepton pair peak very sharply for small κ^2, thereby favoring the Higgs-boson case. On the other hand, the hypercolor-mesons signal will be swamped by the above background.

We note in passing that we have concentrated our calculations for $m_H \approx 10$ to 50 GeV/c^2. Above $m_H = 50$ GeV/c^2 the branching ratio for reaction (1.1) will be too small for LEP and SLC to detect the Higgs boson. Below 10 GeV/c^2 the decays of Υ will be a better signal provided we can accumulate enough events. It is interesting to note that for $m_H \lesssim 10$ GeV/c^2, reaction (1.1), we have a different signal for H^0 production. In this event for $l^{\pm}=\mu^{\pm}$ we will have a peak in the Q^2 distribution at $Q^2=m_H{}^2$ and the two quarks will form hadrons or two jets with no distinct mass peaks. However, we believe this range will be adequately covered by the Cornell Electron Storage Ring and DORIS in the near future.

In conclusion, the decay (1.1) of the Z^0 is a very good reaction to search for elementary Higgs bosons for $10 < m_H \lesssim 50$ GeV/c^2. Once found the decay spectra can be used to determine its parity and distinguishing it from hypercolor mesons and composite mesons is also possible.

[1]G. Arnison *et al.*, Phys. Lett. 126B, 398 (1983).
[2]S. Weinberg, Phys. Rev. Lett. 19, 1264 (1976); A. Salam and J. C. Ward, Phys. Lett. 13, 108 (1964); S. L. Glashow, Nucl. Phys. 22, 579 (1961).
[3]A. Sirlin and W. J. Marciano, Nucl. Phys. B189, 442 (1981).
[4]C. H. Llewellyn Smith and J. F. Wheater, Phys. Lett. 105B, 486 (1981).
[5]S. Weinberg, Phys. Rev. D 13, 974 (1976); 19, 1277 (1979); L. Susskind, *ibid.* 20, 2619 (1979). For a review, see E. Farhi and L. Susskind, Phys. Rep. 74, 277 (1981).
[6]F. M. Renard, Phys. Lett. 126B, 59 (1983); 116B, 269 (1982); Nucl. Phys. B196, 93 (1982).
[7]J. D. Bjorken, in *Weak Interactions at High Energy and the Production of New Particles,* proceedings of SLAC Summer Institute on Particle Physics, 1976, edited by M. Zipf (Report No. SLAC-198, 1977).
[8]E. Ma and J. Okada, Phys. Rev. D 20, 1052 (1979).
[9]A. Ali and M. A. B. Bég, Phys. Lett. 103B, 376 (1981).
[10]J. Ellis, M. K. Gaillard, D. V. Nanopoulos, and P. Sikivie, Nucl. Phys. B182, 529 (1981); S. Dimopoulos, S. Raby, and G. L. Kane, *ibid.* B182, 77 (1981).
[11]G. Barbiellini *et al.*, Report No. DESY 79/27, 1979 (unpublished).
[12]G. Ekspong and K. Hultqvist, University of Stockholm, Institute of Physics, Report No. 82-05, 1982 (unpublished).